Experimental studies of far-field superlens for sub-diffractional optical imaging

Zhaowei Liu, Stéphane Durant†, Hyesog Lee, Yuri Pikus, Yi Xiong, Cheng Sun and Xiang Zhang*

5130 Etcheverry Hall, NSF Nanoscale Science and Engineering Center (NSEC), University of California, Berkeley, California, 94720

xiang@berkeley.edu

http://xlab.me.berkeley.edu

Abstract: Contrary to the conventional near-field superlensing, subwavelength superlens imaging is experimentally demonstrated in the far-field. The key element is termed as a Far-field SuperLens (FSL) which consists of a conventional superlens and a nanoscale coupler. The evanescent fields from the object are enhanced and then converted into propagating fields by the FSL. By only measuring the propagating field in the far-field, the object image can be reconstructed with subwavelength resolution. As an example of this concept, we design and fabricate a silver structured one dimensional FSL. Experimental results show that feature resolution of better than 50nm is possible using current FSL design. © 2007

OCIS codes: (110.0180) Microscopy; (240.6680) Surface Plasmons; (350.7420) Waves.

References and links:

1. M. Born, and E. Wolf, *Principles of Optics* (Pergamon Press, Fourth edition 1970).
2. E. Betzig, J. K. Trautman, T. D. Harris, J. S. Weiner, and R. K. Kostelak, "Breaking the diffraction barrier: optical microscopy on a nanometric scale," Science **251**, 1468-1470 (1991).
3. D. Courjon, *Near-field microscopy and near-field optics* (London, Imperial College Press, 2003).
4. S. W. Hell and J. Wichmann, "Breaking the diffraction resolution limit by stimulated emission: stimulated emission deletion microscopy," Opt. Lett. **19**, 780-782 (1994).
5. S. W. Hell, "Toward fluorescence nanoscopy," Nat. Biotechnol. **21**, 1347-1355 (2003).
6. R. Heintzmann, T. M. Jovin, and C. Cremer, "Saturated patterned excitation microscopy-a concept for optical resolution improvement," J. Opt. Soc. Am. A **19**, 1599-1609 (2002).
7. M. G. L. Gustafsson, "Nonlinear structured-illumination microscopy: Wide-field fluorescence imaging with theoretically unlimited resolution," PNAS **102**, 13081-13086 (2005).
8. M. J. Rust, M. Bates, and X. W. Zhuang, "Sub-diffraction-limit imaging by stochastic optical reconstruction microscopy (STORM)," Nature Method **3**, 793-795 (2006).
9. E. Betzig, G. H. Patterson, R. Sougrat, O. W. Lindwasser, S. Olenych, J. S. Bonifacino, M. W. Davidson, J. Lippincott-Schwartz, and H. F. Hess, "Imaging intracellular fluorescent proteins at nanometer resolution," Science **313**, 1642-1645 (2006).
10. J. Gelles, B. J. Schnapp, and M. P. Sheetz, "Tracking kinesin-driven movements with nanometer-scale precision," Nature **331**, 450–453 (1988).
11. A. Yildiz, J. N. Forkey, S. A. Mckinney, T. Ha, Y. E. Goldman, P. R. Selvin, "Myosin V walks hand-over-hand: Single fluorophore imaging with 1.5-nm localization," Science **300**, 2061–2065 (2003).
12. J. B. Pendry, "Negative refraction makes a perfect lens," Phys. Rev. Lett. **85**, 3966-3969 (2000).
13. C. G. Parazzoli, R. B. Greegor, K. Li, B. E. C. Koltenbah, M. Tanielian, "Experimental verification and simulation of negative index of refraction using Snell's law," Phys. Rev. Lett. **90**, 107401 (2003).
14. A. A. Houck, J. B. Brock, and I. L. Chuang, "Experimental observations of a left-Handed material that obeys Snell's law," Phys. Rev. Lett. **90**, 137401 (2003).
15. A. Grbic and G. V. Eleftheriades, "Overcoming the diffraction limit with a planar left-handed transmission-line lens," Phys. Rev. Lett. **92**, 117403 (2004).
16. W. Cai, D. A. Genov, and V. M. Shalaev, "A superlens based on metal-dielectric composites," Phys. Rev. B **72**, 193101 (2005).
17. C. Luo, S. G. Johnson, J. D. Joannopoulos, and J. B. Pendry, "Subwavelength imaging in photonic crystals," Phys. Rev. B **68**, 045115 (2003).

#80750 - $15.00 USD Received 6 Mar 2007; revised 18 Apr 2007; accepted 21 Apr 2007; published 22 May 2007

18. V. P. Parimi, W. T. Lu, P. Vodo, and S. Sridhar, "Photonic crystals – imaging by flat lens using negative refraction," Nature **426**, 404-404 (2003).
19. E. Cubukcu, K. Aydin, E. Ozbay, S. Foteinopou, C. M. Soukoulis, "Subwavelength resolution in a two-dimensional photonic-crystal-based superlens," Phys. Rev. Lett. **91**, 207401 (2003).
20. N. Fang, H. Lee, C. Sun, and X. Zhang, "Sub-diffraction-limited optical imaging with a silver superlens," Science **308**, 534-537 (2005).
21. H. Lee, Y. Xiong, N. Fang, W. Srituravanich, S. Durant, M. Ambati, C. Sun, and X. Zhang, "Realization of optical superlens imaging below the diffraction limit," New J. Phys. **7**, 255, (2005).
22. T. Taubner, D. Korobkin, Y. Urzhumov, G. Shvets, R. Hillenbrand, "Near-field microscopy through a SiC superlens," Science **313**, 1595 (2006).
23. V. A. Podolskiy and E. E. Narimanov, "Near-sighted superlens," Opt. Lett. **30**, 75-77 (2005).
24. S. Durant, Z. Liu, N. Fang, and X. Zhang, www.arxiv.org, physics/0601163, 2006; S. Durant, Z. Liu, J. M. Steele, and X. Zhang, "Theory of the transmission properties of an optical far-field superlens for imaging beyond the diffraction limit," J. Opt. Soc. Am. B **23**, 2383-2392 (2006).
25. Z. Liu, S. Durant, H. Lee, Y. Pikus, Y. Xiong, C. Sun, and X. Zhang, X., "Far-field optical superlens," Nano. Lett. **7**, 403-408 (2007).
26. Z. Jacob, L. V. Alekseyev, and E. Narimanov, "Optical hyperlens: Far-field imaging beyond the diffraction limit," Opt. Express **14**, 8247-8256 (2006).
27. A. Salandrino and N. Engheta, "Far-field subdiffraction optical microscopy using metamaterial crystals: Theory and simulations," Phy. Rev. B **74**, 075103 (2006).
28. Z. Liu, H. Lee, Y. Xiong, C. Sun, and X. Zhang, "Optical hyperlens magnifying sub-diffraction-limitted object," Science **315**, 1686 (2007).
29. Z. Liu, S. Durant, H. Lee, Y. Xiong, Y. Pikus, C. Sun, and X. Zhang, "Near-field Moire effect mediated by surface plasmon polariton excitation," Opt. Lett. **32**, 629-631 (2007).
30. M. G. L. Gustafsson, "Surpassing the lateral resolution limit by a factor of two using structured illumination microscopy," J. Microsc.-Oxf **198**, 82-87 (2000).
31. J. T. Frohn, H. F. Knapp, and A. Stemmer, "True optical resolution beyond the Rayleigh limit achieved by standing wave illumination," PNAS **97**, 7232-7236 (2000).
32. V. Krishnamurthi, B. Bailey, and F. Lanni, "Image processing in 3-D standing-wave fluorescence microscopy," Proc. SPIE Int. Soc. Opt. Eng. **2655**, 18 (1996).
33. M. A. Grimm and A. W. Lohmann, "Superresolution image for one-dimensional objects," J. Opt. Soc. Am. **56**, 1151-1156 (1966).
34. M. G. Moharam, E. B. Grann, D. A. Pommet, and T. K. Gaylord, "Formulation for stable and efficient implementation of the rigorous coupled-wave analysis of binary gratings," J. Opt. Soc. Am. A **12**, 1068-1076 (1995).

1. Introduction

The resolution of classical optical microscopes is always limited by the so-called diffraction limit due to the wave nature of light [1]. The smallest resolvable distance is given by $\Delta r=\lambda/2n\sin(\theta)$, where λ is the working wavelength in free space, n is the refractive index of the surrounding medium, and θ is the collection angle of the imaging optics. Even though the resolution can be improved by replacing materials with larger n, this improvement is rather modest owing to the availability of such materials.

To overcome the diffraction limit and achieve nanoscale optical imaging, a straight-forward way is to detect the optical signal in the near-field of the object. Near-field scanning optical microscopy (NSOM) [2, 3], one of the most popular techniques so far, forms its image by scanning an ultra sharp tip in the vicinity of the object and collecting signal point by point. Instead of a physical tip, another family of methods based on a virtual light probe has also been developed. Stimulated emission depletion (STED) fluorescence microscopy [4, 5] and saturated structured-illumination microscopy (SSIM) [6, 7] utilize a tiny light spot or line to scan the samples. Nonlinear response of the materials shrinks the light spot size or linewidth into deep subwavelength scale achieving nanoscale spatial resolution. Single-molecule positioning can achieve almost arbitrarily high accuracy if a sufficient number of photons are collected [8, 9]. By aggregating a series of position information, a super-resolution image can also be assembled [10, 11]. All of the aforementioned techniques have shown great success in nanoscale imaging despite the associated limitations.

Another imaging strategy, which is called superlens imaging, recently is receiving a lot of attentions due to its inherent high resolution and real time imaging ability. The concept was

#80750 - $15.00 USD Received 6 Mar 2007; revised 18 Apr 2007; accepted 21 Apr 2007; published 22 May 2007

first proposed in 2000 [12]. Rather than just detecting evanescent waves before decaying as in NSOM, superlens can enhance evanescent waves to compensate the decay which leads to a high resolution image. The superlens theory was then experimentally proved with a wide spectrum of frequency in composite metamaterials [13-16], photonic crystals [17-19], and most recently in natural silver [20, 21] and SiC film [22]. However, all the superlens experimental demonstrations so far are limited to near-field image projection originating from the very underlying principle of the superlens [12, 23]. One has to use either photoresist exposure method [20, 21] or near-field scanning method [22] to record this image which considerably limits the potential applications for this exciting imaging scheme. The far-field superlensing concept, directly interfaced with conventional optics and image recording instruments, enables real time high resolution optical imaging possibility, which is in great demands. Recent far-field optical superlens [24, 25] and optical hyperlens [26-28] has shown exciting advancement in this direction. By designing a metamaterial lens with hyperbolic dispersion, a hyperlens is able to magnify a sub-diffraction-limited object into a diffraction-limited image which allows the far-field detection. The first optical hyerlens has been experimentally demonstrated most recently using a metal/dielectrics multilayer structure [28]. On the other hand, by taking advantage of planar geometry and the evanescent-to-propagating wave conversion by a nanograting, a far-field superlens (FSL) can not only obtain sub-diffraction limited image in the far-field but also with a very large view size [24, 25]. In this paper, we present a specific experimental study of a simplified one-dimensional (1D) FSL for 1D object imaging using the principle of moiré effect. The experimental result shows that this silver structured FSL has approximately 3 fold resolution enhancement in far-field comparing with conventional optical lenses.

2. One dimensional FSL for far-field subwavelength imaging

A FSL consists of a slab superlens and a nanoscale grating coupler. If the coupler is brought to the vicinity of the superlens thus overlapped with the near-field image, a moiré fringe pattern is constructed (see the schematic representation in Fig. 1). This pattern can be understood by a near-field moiré effect [29] due to evanescent wave "frequency mixing" between the superposed near-field image and the grating. By translating unresolvable high spatial frequency into low spatial frequency moiré fringes, the high resolution information of the object becomes detectable in the far-field. The sub-diffraction limited image can be subsequently reconstructed by using far-field measurement data. This is the physical foundation of the resolution extension of the FSL.

If the grating contains a spatial frequency $\mathbf{k}_\Lambda$, the image (projected by a superlens in the near-field) frequency $\mathbf{k}$ gives rise to moiré fringes at frequency $\mathbf{k}$-$\mathbf{k}_\Lambda$. Those fringes can be observed by conventional optical microscope if $\mathbf{k}$-$\mathbf{k}_\Lambda$ lies in the observable range ($|\mathbf{k}$-$\mathbf{k}_\Lambda|<k_{obs}$). Therefore, the highest observable spatial frequency (the resolution) in Fourier space is extended from k_{obs} to $k_{obs}+k_\Lambda$ (Fig. 2). In return, the information obtained in the observable circle is the sum of three components from different diffraction orders of the grating. It is worth emphasizing that k_Λ is only limited by the grating geometry while k_Λ in structured illumination [30, 31] is limited by diffraction limit.

#80750 - $15.00 USD Received 6 Mar 2007; revised 18 Apr 2007; accepted 21 Apr 2007; published 22 May 2007

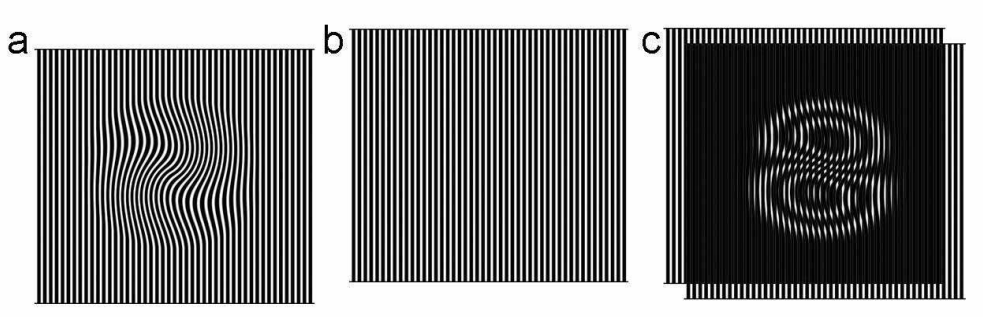

Fig. 1. Improve the far-field resolvability by near-field moiré effect. (a) The near-field optical image of the object. (b) Subwavelength coupling grating. (c) Far-field observable moiré fringes by superposing (a) and (b). The original object image can be numerically restored from the moiré fringes with subwavelength resolution.

In order to obtain a high resolution image, the three overlapped frequency components have to be separated and relocated to its original position. This can be done by taking multiple measurements with relative phase-shift between the object and the grating and followed by a data processing procedure [32]. As the object and the grating are in each other's near-field, very complicated instruments are needed to translate a grating over the object with nanometer precision. In addition, the objects must keep unchanged during the time of translation which makes this method unsuitable for real time high speed imaging. To solve the wavevector mixing issue without the translation process, a FSL with specific wavevector dependent optical transfer function (OTF) provide a completely new approach [24, 25]. According to the desired OTF, only one diffraction order can go through the FSL which enables the "one-to-one" relationship between the detectable propagating wave and its evanescent origin. However, under certain specific cases, (such as the object is 1D as shown in Fig. 2. the spectrum of the object is a straight line), the different diffraction orders can not only be shifted into the detectable region but also be separated in space by introducing a small angular misalignment between the 1D object and the 1D grating (Fig. 2). To avoid the overlapping between diffraction orders, the width of the spectrum has to be smaller than the displacement of the first order along y direction. The displacement however can not be too large; otherwise the first order band will be clipped by the circle of the observable domain. Therefore, the total length of the testing object along y direction, the periodicity of the coupling grating and also the misalignment angle need to be properly pre-examined.

With the help of the second dimension rather than the OTF, the retrievable 1D object information can be extended by relocating the detected different diffraction orders within the far-field detectable region (the detected signal is just moiré fringes in real space). Since there is no need of multiple detections, it is more suitable for 1D real time imaging with super resolution. The resolution is fundamentally determined by how many orders can be effectively utilized to couple evanescent waves into propagating ones. We only show the first order coupling to explain the principle, but the concept is not limited by that.

The waves coupled by diffractions of a subwavelength grating are evanescent. Any distance between the object and the coupling grating may lead to significant field amplitude loss. In addition, the amplitude of higher spatial frequency is usually smaller for a natural object. As a consequence, the high order information is extremely weak which also means the contrast of the moiré fringes is very low. The contrast of the moiré fringes, however, can be dramatically enhanced by the surface plasmon excitation on a silver superlens as we discussed in our previous paper [29]. Therefore, a FSL (i.e. both a superlens and a grating), instead of a simple grating [33], has to be used to enhance the imaging performance when evanescent waves are involved.

#80750 - $15.00 USD Received 6 Mar 2007; revised 18 Apr 2007; accepted 21 Apr 2007; published 22 May 2007

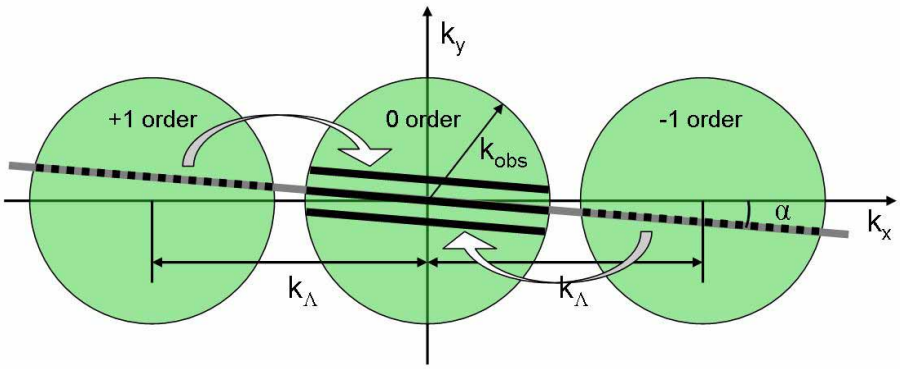

Fig. 2. The concept of a simplified 1D far-field superlens (FSL). The accessible area of a conventional optical lens in Fourier space is defined by the central circle with radius k_{obs} (k_{obs} is limited to propagating wave). A FSL can shift original evanescent waves to propagating waves by its diffraction orders. If the object is also 1D and has an angular misalignment α with respect to the grating of the FSL, the object information goes through different diffraction orders will be separated in space. By this way, the maximum spatial frequency that can be detected and restored is $k_{obs}+k_{\Lambda}$.

The OTF of one exampled silver structured FSL is calculated by a rigorous coupled wave analysis (RCWA) method [34] and shown in Fig. 3. The OTF presents remarkable enhancement with large spatial frequencies (wave vector) but suppression for small spatial frequencies which will results in a great contrast improvement in both moiré fringes and the final restored high resolution images. Now, the remaining issue is to measure the enhanced moiré pattern and restore the image with subwavelength resolution.

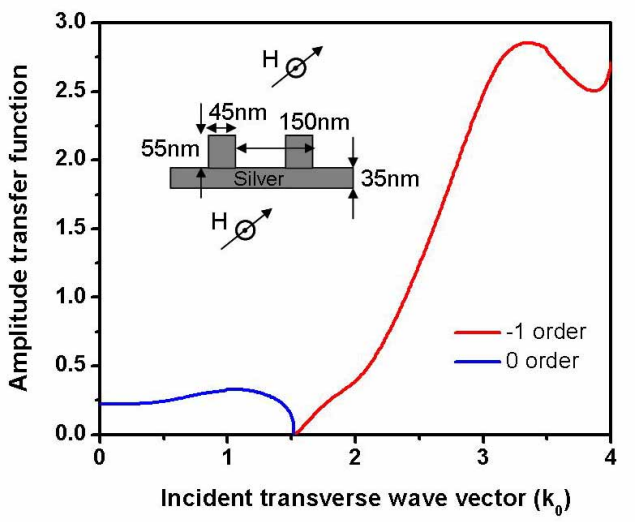

Fig. 3. The optical amplitude transfer function (ATF) of a structured silver FSL (only propagating wave is shown) for TM mode. The FSL geometries are shown in the inset. The refractive index of the surrounding medium is set to 1.52 and the working light wavelength is 377nm in vacuum

#80750 - $15.00 USD Received 6 Mar 2007; revised 18 Apr 2007; accepted 21 Apr 2007; published 22 May 2007

3. Experimental methods and results

We fabricated a combo sample comprising of both a line object and a 1D FSL. The sample fabrication started with a 40nm chrome film deposition on a quartz wafer. Slits, which were served as objects, were then etched through the Cr film using focused ion beam (FIB, Strata 201XP). The length of the slits was approximately 14μm. In order to realize a flat bottom surface of the FSL which is shown in Fig. 3 inset, 35nm PMMA planarized film spacing layer is required to eliminate the surface modulations of the Cr object. This layer must also be thin enough to prevent significant decay of the evanescent waves generated by the objects. The planarization process started from a thick spin-coated PMMA layer (~700nm), followed by plasma etching processes to reduce the thickness down to ~35nm. The final thickness of PMMA was measured by a FilmTek 2000 film thickness monitor. This process promises a flat PMMA surface with better than 1nm roughness.

The FSL fabrication is comprised of three major steps. First, a 35nm silver film was deposited on top of a planarized PMMA layer. Secondly, A 100nm thick PMMA layer was spin coated, E-beam patterned and developed as a grating (150nm periodicity with 45nm opening). The relative position between the FSL and the object was well controlled by aligning both of them with respect to a fixed alignment mark on the substrate. The angle between the object and the FSL is around 3°. Finally, additional 55nm silver film was deposited and then followed by a lift-off process. The additional silver grating before the lift-off process can decrease the total transmission light but increase the OTF ratio between first order and zero order as well. In our previous work [25], the separation of the mixed wavevectors depends on the ratio of the OTF, therefore, there is no need of the lift-off process. In current work, we utilize the second dimension to separate the mixed wavevectors, the requirement of the OTF is much more relaxed thus we prefer to remove the additional silver grating to improve the transmittance and also the signal to noise ratio. An E-beam evaporator (SLOAN) was used for all of the metallic film depositions under high vacuum. The total area of the silver FSL is 50μm×50μm, which assures that a FSL can completely cover an object. The final FSL was characterized by both scanning electron microscope (SEM) and atomic force microscope (AFM) (see Fig. 4). All of the dimensions are proximately equal to desired values.

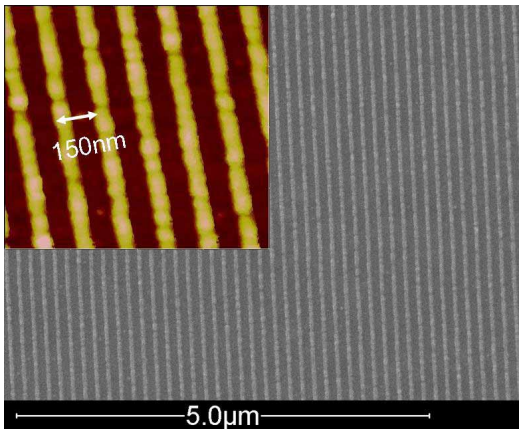

Fig. 4. Scanning electron microscope (SEM) image of the silver structured FSL. The dimensions are the same as shown in Fig. 3 inset. Inset: a zoom-in atomic force microscope (AFM) image shows the grating height is also quite uniform. The ridge width in AFM image is little bit larger than that in SEM image due to the finite size of the AFM tip.

#80750 - $15.00 USD Received 6 Mar 2007; revised 18 Apr 2007; accepted 21 Apr 2007; published 22 May 2007

The sample was measured by an optical microscope (Zeiss Axiovert mat 200, 100X oil immersion objective, N.A. =1.4) under normally incident *p* polarized light at 377 nm wavelength (coherent RADIUS 375-8). The far-field images were recorded using a UV sensitive CCD camera (Princeton Instruments VersArray 1300F). Under these conditions (k_{obs}=1.4k_0, $k_\Lambda \approx 2.5k_0$), the observable spatial frequency can go up to 3.9k_0. The orders are well separated but not far away from the center of the observable circle considering the object length (~14 μm), grating period (150nm), and also the misalignment angle (3º).

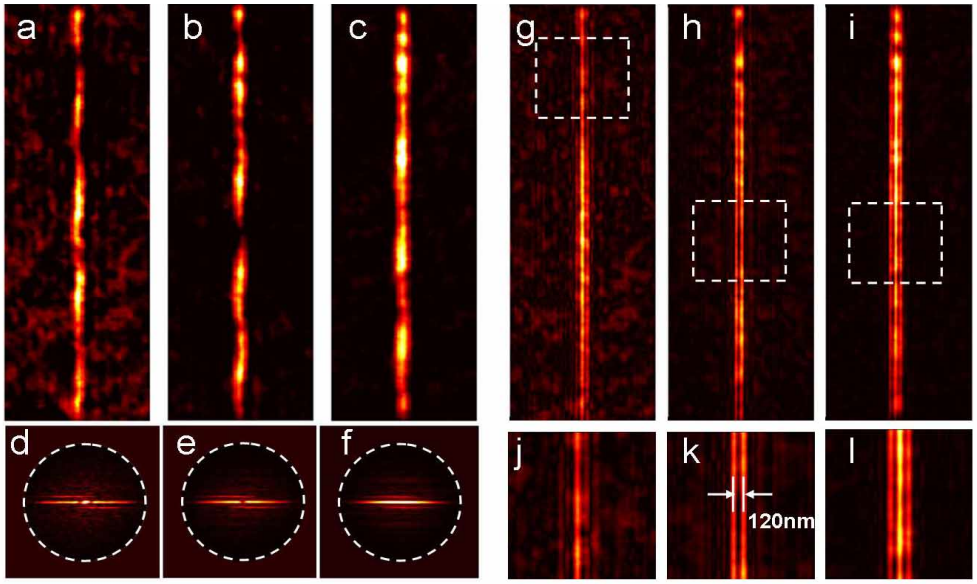

Fig. 5. Directional FSL images of (a) single-line object with 50nm linewidth; (b) double-line object with 50nm linewidth and 70nm edge-to-edge distance; (c) triple-line object with 50nm linewidth and 70nm edge-to-edge distance. (d), (e), and (f) 2D Fourier transformation of (a), (b), and (c) respectively. The area within the white circle represents the far-field detectable information (NA≤1.4) by the optical microscope. (g), (h), and (i) Reconstructed images from (d), (e), and (f) respectively. (j), (k), and (l) zoom-in view of the dashed white rectangle area in (g), (h), and (i) respectively.

In order to obtain the object image with resolution below the diffraction limit, a straightforward image reconstruction procedure was used. As an example, we show the image reconstruction process by using test slit objects with 50nm opening and 70nm edge-to-edge distance. The direct optical microscopy image obtained by *p*-polarized illumination is shown in Figs. 5(a), 5(b), and 5(c) for single, double, and triple slit respectively. We did 2D Fourier transformation for those images and their spectra are shown in Figs. 5 (d), 5(e), and 5(f). Since the line pair object was purposely oriented with a small angle with respect to the grating direction of the FSL. The resulting different orders of transmission through the FSL were separated in Fourier spectrum. The 0, +1, and -1 FSL diffraction order can be clearly seen from Figs. 5 (d), 5(e), and 5(f), which is consistent with our expectation as shown in Fig. 2. The +1 and -1 order that carry the subwavelength information can be shifted back (reverse the big white arrow direction in Fig. 2) with the given wavevector of the FSL and angle between the FSL and the object. Subsequently, inversed Fourier transformation is performed and the reconstructed object image is shown in Figs. 5(g), 5(h), and 5(i). From the zoom-in view of the reconstructed images [Figs. 5(j), 5(k), and 5(l)], all of the three subwavelength object were clearly resolved. The feature size resolution is around 50nm. Comparing with the case without FSL (feature size resolution ~ 135nm for NA=1.4), our FSL experiment shows about

#80750 - $15.00 USD Received 6 Mar 2007; revised 18 Apr 2007; accepted 21 Apr 2007; published 22 May 2007

3 fold resolution improvement. Note that the increase of the total light transmittance can drastically improve the signal to noise ratio in both directional measurement data and the reconstructed images. To further demonstrate the imaging ability of the FSL, we also tested a triple line object with 50nm linewidth and various edge-to-edge distances (60nm, 80nm, and 100nm). The directional optical images and the reconstructed images are presented in Fig. 6. Obviously, all of the three lines of the objects are resolved with great fidelity. The difference in slit distances among the objects, as small as 20nm, has been clearly distinguished.

The numerical image reconstruction process only comprises Fourier transformations and image lateral shift. It is much simpler and more straightforward comparing with the very complicated reconstruction algorithm of MRI and X-ray crystallography. In fact, such a simple reconstruction process can be performed completely by optical components. For instance, Fourier transformation can be achieved by a lens; while lateral shift can be done by a grating. We will discuss more details about the optical reconstruction elsewhere.

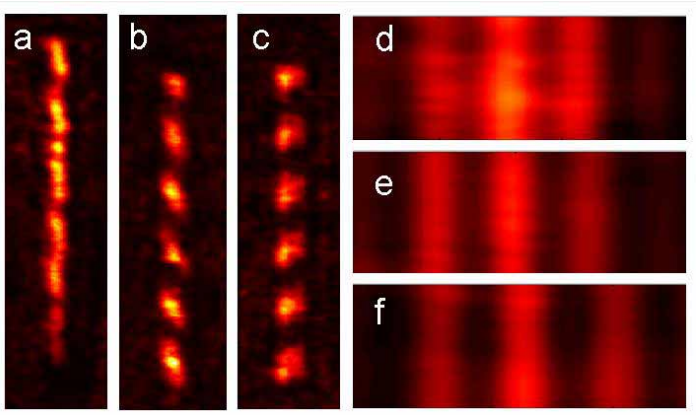

Fig. 6. Directional FSL images of a triple-line object with 50nm linewidth and (a) 60nm (b) 80nm and (c) 100nm edge-to-edge distance. (d), (e), and (f) Zoom-in view of the reconstructed images for object (a), (b) and (c) respectively.

4. Conclusions

In conclusion, we have experimentally demonstrated the far-field imaging ability of a 1D silver structured FSL. Working at 377nm vacuum wavelength, 50nm features with 20nm difference have been clearly resolved. Comparing with the conventional diffraction limited optics, our current design of the FSL shows 3 fold resolution improvement.

Acknowledgments

This research was supported by the Center for Scalable and Integrated Nanomanufacturing (SINAM), an NSF Nanoscale Science and Engineering Center (NSEC) under award number DMI-0327077, and Office of Naval Research (ONR)/Defense Advanced Research Projects Agency Multidisciplinary University Research Initiative (MURI) (ONR grant N0014-01-1-0803).

† Stéphane Durant's present address: KLA-Tencor Corp., 1 Technology Dr, Milpitas, CA 95035, USA

#80750 - $15.00 USD Received 6 Mar 2007; revised 18 Apr 2007; accepted 21 Apr 2007; published 22 May 2007